Spatially and Temporally Correlated MIMO Channels: Modeling and Capacity Analysis

Geoffrey J. Byers, *Student Member, IEEE,* and Fambirai Takawira, *Member, IEEE*

Abstract—Wireless communication systems employing multiple antennas at both the transmitter and receiver have been shown to offer significant gains over single-antenna systems. Recent studies on the capacity of multiple-input–multiple-output (MIMO) channels have focused on the effect of spatial correlation. The joint effect of spatial and temporal correlation has not been well studied. In this paper, a geometric MIMO channel model is presented, which considers motion of the receiver and nonisotropic scattering at both ends of the radio link. A joint space–time cross-correlation function is derived from this model and variates with this joint correlation are generated by using the vector autoregressive stochastic model. The outage capacity of this channel is considered where the effects of antenna spacing, antenna array angle, degree of nonisotropic scattering, and receiver motion are investigated. When n transmit and n receive antennas are employed, it is shown that the outage capacity still increases linearly with respect to n, despite the presence of spatial and temporal correlation. Furthermore, analytical expressions are derived for the ergodic capacity of a MIMO channel for the cases of spatial correlation at one end and at both ends of the radio link. The latter case does not lend itself to numerical evaluation, but the former case is shown to be accurate by comparison with simulation results. The proposed analysis is very general, as it is based on the transmit and receive antenna correlations matrices.

Index Terms—Ergodic capacity, fading channels, multiple-input–multiple-output (MIMO) systems, multielement antenna systems, outage capacity, space–time correlation.

I. INTRODUCTION

WITH the increasing demand for high-data-rate wireless communication services coupled with the problem of power and bandwidth restrictions, as well as the harsh multipath fading channel, the field of high-data-rate, spectrally efficient, and reliable wireless communications is currently receiving much attention.

It was shown in [1] and [2] that multiple-input–multiple-output (MIMO) channels, whereby multiple antennas are employed at both the transmitter and receiver, offer large gains in capacity over single-input–single-output (SISO) channels. In order to exploit the benefits of MIMO channels, various coding schemes have been developed, which include layered space–time codes [3], space–time trellis codes [4], and space–time block codes [5].

A common communications scenario is one in which the base station is elevated and unobstructed by local scatterers and the signal is received within a given beamwidth. The user is situated at ground level, where a high degree of local scattering occurs due to objects surrounding the user. The effect of spatial correlation in such a channel on MIMO capacity was investigated in [6],[7], and in [8], where nonisotropic scattering at the user was also considered.

Another common scenario occurs when both the transmitter and receiver are surrounded by objects, resulting in local scattering at both ends of the radio link. The channel capacity of this channel was considered in [9]–[11], but the effects of user mobility on channel capacity were not investigated.

The effect of user mobility, resulting in temporal correlation, on the capacity of MIMO channels is becoming increasingly important as future communication systems are expected to operate at high data rates and high mobility. However, the capacity of MIMO channels with user mobility and local scattering at both ends of the radio link has not been well studied.

In order to study the capacity of the channel described, one can perform a number of field measurements from which the capacity can be calculated. MIMO field measurements have been performed by a number of authors for indoor [12]–[15], outdoor-to-indoor [16], and outdoor environments [17]–[20]. In several cases, capacities close to the theoretical case were obtained. However, capacity results obtained in this manner are only applicable to a particular environment and array configuration. Furthermore, it is difficult to study the effect of particular parameters, such as angle spread, on MIMO capacity.

An excellent overview of MIMO channel models is given in [21]. These models can be classified as field-measurement or scatterer models. Field-measurement models [16], [20] are preferable, as they are based on measurement data and give an accurate model of the environment under study. However, scatterer or geometric models are more flexible and give a good description of the communications channel. These models are simple and allow the main characteristics of the channel to be studied without the need for time-consuming field measurements. Geometric models have been used to model single-antenna systems [22], [23] and systems with multiple antennas at one end of the radio link [24]–[28]. Geometric models for MIMO systems with local scattering at one end [6]–[8], [29] and both ends of the radio link [9], [10], [29] are available in the literature. However, only the model of [9] considered local scattering at both ends of the radio link as well as user mobility, but this model requires lengthly simulations to generate the path gains. What is desired is a closed-form expression for the correlation between paths from which the path gains of the MIMO channel can be efficiently generated.
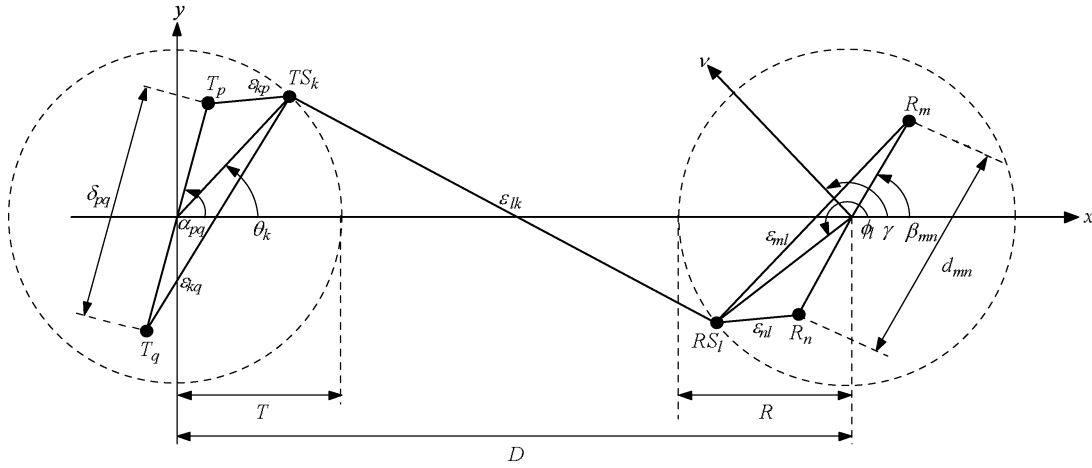
Fig. 1. Geometric model for the MIMO channel with $n_T = n_R = 2$.

This paper presents two main contributions. The first is as follows. A geometric model for a MIMO channel is presented, which accounts for user mobility and nonisotropic scattering at both the transmitter and receiver. From this model, a closed-form joint space–time cross-correlation function is derived. The path gains of this channel are efficiently generated with the desired joint space–time cross-correlation using the vector autoregressive (AR) stochastic model proposed in [30]. The effect of spatial and temporal correlation on the outage capacity of this MIMO channel is then investigated.

The second contribution is the derivation of an exact analytical expression for the ergodic capacity of a MIMO channel, where spatial correlation is present at one end and at both ends of the radio link. The capacity of MIMO channels is generally investigated using simulation-based methods due to the difficulty experienced in deriving analytical expressions. Where analytical expressions have been investigated, the ergodic capacity, rather than the outage capacity, was considered, as the latter is more complicated mathematically. In [1], an analytical expression was derived for the ergodic capacity of an uncorrelated MIMO channel, which was then evaluated using numerical integration. Most authors have proposed bounds on or approximations to the ergodic capacity, as exact expressions are more difficult to derive. Approximations and bounds were investigated in [2] and [31]–[34] for the case of no correlation and in [6], [7], [35], and [36] for the case of spatial correlation at one end of the radio link. To the extent of the authors' knowledge, no exact analytical expression has been derived for the case of spatial correlation at one end of the radio link and no analytical expression, bound or approximation, has been derived for the case of spatial correlation at both ends of the radio link.

The paper is arranged as follows. The geometric MIMO channel model is presented in Section II and the corresponding joint space–time cross-correlation function is derived in Section III. Simulation results validating aspects of the model and investigating the outage capacity of this channel are presented in Section IV. Analytical expressions are derived for the ergodic capacity of a MIMO channel with spatial correlation at one end and at both ends of the radio link in Section V. The accuracy of this analysis is validated in Section VI by a comparison with simulation results. Finally, conclusions are drawn in Section VII.

II. MIMO CHANNEL MODEL

Consider a narrow-band single-user communications system with n_T transmit and n_R receive omnidirectional antenna elements. It is assumed that there is no line of sight (LoS) between the transmitter and receiver and that the fading is caused by scatterers at both ends of the radio link. Only local scattering is considered, as it is assumed that the path loss will limit the contribution of remote scatterers to the total channel energy. The transmitter is taken to be fixed and the receiver is taken to be moving.

The link between the transmit and receive antenna arrays is represented using the complex baseband vector notation

$$\underline{y}(t) = \boldsymbol{H}(t)\underline{x}(t) + \underline{n}(t). \tag{1}$$

The $n_T \times 1$ transmit vector $\underline{x}(t)$ has elements $x_j(t)$, which denote the signal transmitted from antenna $j = \{1, \ldots, n_T\}$. The $n_R \times 1$ receive vector $\underline{y}(t)$ has elements $y_i(t)$, which denote the signal received on antenna $i = \{1, \ldots, n_R\}$. The $n_R \times 1$ noise vector $\underline{n}(t)$ has elements $n_i(t)$, which denote the additive white Gaussian noise (AWGN) at receiver branch i. Finally, $\boldsymbol{H}(t)$ is the $n_R \times n_T$ channel matrix of complex path gains $h_{ij}(t)$ between transmit antenna j and receive antenna i.

The entries of the noise vector are independent and identically distributed (i.i.d.) complex Gaussian-random variables with variance N_0, where N_0 is the noise power spectral density. It is assumed that the channel is known to the receiver and unknown to the transmitter, which must equally divide the total transmit power over all antennas.

In Fig. 1, a geometric model for the MIMO channel under consideration is presented, where $n_T = n_R = 2$. This general structure can be used to represent any array configuration. The distance between the transmitter and receiver arrays is D. The geometric model presented here is the two-ring model, which has been considered by a number of authors [9], [10], [21], [26], [29] to model local scattering at both the transmitter and receiver. The two-ring model is a generalization of the classic one-ring model employed by Jakes [22], where a ring of scatterers is used to model local scattering around the user.

There are K omnidirectional scatterers at the transmitter, which lie on a ring of radius T where the k_{th} transmit scatterer is denoted by TS_k. Similarly, there are L omnidirectional scatterers at the receiver, which lie on a ring of radius R where the l_{th} receive scatterer is denoted by RS_l. Only local scattering is considered, i.e., $T \ll D$, $R \ll D$.

Each scatterer introduces a gain and a phase shift. It is assumed that the gain and phase shift introduced by a particular scatterer is dependent on the direction of the ray's arrival. Thus, the gain and phase shift introduced by RS_l when a ray is received from TS_k is different from that introduced when a ray is received from $TS_{k'}$ where $k \neq k'$. If the antenna spacing is small relative to the scattering radius, it can be assumed that rays from different antenna elements arrive at a particular scatterer at approximately the same angle. Thus, for a particular scatterer, the gain and phase shift is the same for rays arriving from different antenna elements. For this reason, g_{lk} and ψ_{lk} are used to denote the joint gain and phase shift of the scatterers TS_k and RS_l. A similar assumption was made in [9], which avoids the difficulties experienced in the two-ring model discussed in [21]. The scatterer gains are taken to be independent, finite variance, positive random variables that are independent of the scatterer phase shifts. Furthermore, it is assumed that

$$\frac{1}{KL} \sum_{k=1}^{K} \sum_{l=1}^{L} E\left[g_{lk}^2\right] = 1. \tag{2}$$

The scatterer phase shifts are i.i.d. and uniformly distributed over the interval $[0, 2\pi)$.

Both scattering rings are assumed to be fixed and the motion of the receiver is modeled by a speed ν and a direction γ. By making these assumptions, a stationary cross-correlation function is obtained, as discussed in [8].

Consider a single-transmission path from transmit antenna T_p to receive antenna R_m, where the power transferred through this link is Ω_{mp}. The plane waves transmitted from antenna T_p are scattered by the transmit scatterers and then by the receive scatterers, which results in many rays impinging on antenna R_m. The channel gain $h_{mp}(t)$ for the $T_p - R_m$ link, considering the contributions of all scatterers, can be represented as

$$h_{mp}(t) = \sqrt{\Omega_{mp}} \lim_{K,L \to \infty} \frac{1}{\sqrt{KL}} \sum_{k=1}^{K} \sum_{l=1}^{L} g_{lk}$$
$$\times \exp\left[\jmath \psi_{lk} - \jmath \frac{2\pi}{\lambda}(\varepsilon_{kp} + \varepsilon_{lk} + \varepsilon_{ml})\right.$$
$$\left. + \jmath 2\pi f_D \cos(\phi_l - \gamma)t\right]. \tag{3}$$

Here, ε_{kp}, ε_{lk}, and ε_{ml} are the distances as shown in Fig. 1, λ is the carrier wavelength, $f_D = \nu/\lambda$ is the maximum Doppler frequency, and $\jmath = \sqrt{-1}$.

Given the statistical properties of the channel, the central limit theorem states that $h_{mp}(t)$ is a zero-mean complex Gaussian-random process. Therefore, the envelope of $|h_{mp}(t)|$ is a Rayleigh-fading process.

III. SPACE–TIME CROSS-CORRELATION FUNCTION

In this section, the joint space–time cross-correlation function for the channel presented in Section II is derived in a similar manner to [8]. This cross-correlation function is then compared to correlation results in the literature in order to assess the validity of the channel.

The correlation between the two links, $T_p - R_m$ and $T_q - R_n$, for a time delay τ is defined as

$$\rho_{mp,nq}(t,\tau) = \rho_{mp,nq}(\tau) = \frac{E\left[h_{mp}(t)h_{nq}^*(t+\tau)\right]}{\sqrt{\Omega_{mp}\Omega_{nq}}} \tag{4}$$

where * is the complex conjugate. This expression defines the spatial correlation between transmission paths, which is related to the temporal correlation over time if the receiver is moving.

The space-time cross-correlation can now be calculated and after some cancellation of terms, can be expressed as

$$\rho_{mp,nq}(\tau) = \lim_{K,L \to \infty} \frac{1}{KL} \sum_{k=1}^{K} \sum_{l=1}^{L} E\left[g_{lk}^2\right]$$
$$\times \exp\left[-\jmath \frac{2\pi}{\lambda}(\varepsilon_{kp} + \varepsilon_{ml} - \varepsilon_{kq} - \varepsilon_{nl})\right.$$
$$\left. - \jmath 2\pi f_D \cos(\phi_l - \gamma)\tau\right]. \tag{5}$$

An important result here is that the correlation between links is independent of the parameter ε_{lk} and, hence, independent of D. In general, (5) must be evaluated using numerical methods. However, by making some approximations, as discussed in this section, a closed-form expression for (5) can be obtained. As the number of scatterers approaches infinity $(K, L \to \infty)$, (5) can be expressed in integral form as

$$\rho_{mp,nq}(\tau) = \int_{-\pi}^{\pi} \int_{-\pi}^{\pi} \exp\left\{-\jmath \frac{2\pi}{\lambda}(\varepsilon_{\theta p} + \varepsilon_{m\phi} - \varepsilon_{\theta q} - \varepsilon_{n\phi})\right.$$
$$\left. - \jmath 2\pi f_D \cos(\phi - \gamma)\tau\right\}$$
$$\times p(\theta)p(\phi)d\theta d\phi \tag{6}$$

where $p(\theta)$ and $p(\phi)$ are the probability distributions of the transmit and receive scatterers, respectively. The term $\varepsilon_{\theta p}$ is the distance from T_p to the point on the transmit-scattering ring at an angle θ from the array center. The other ε terms are defined in a similar fashion.

For a given scatterer distribution, (6) can be calculated numerically using the following equations, which are derived using the law of cosines:

$$\varepsilon_{\theta p}^2 = \frac{\delta_{pq}^2}{4} + T^2 - \delta_{pq}T\cos(\alpha_{pq} - \theta)$$
$$\varepsilon_{\theta q}^2 = \frac{\delta_{pq}^2}{4} + T^2 + \delta_{pq}T\cos(\alpha_{pq} - \theta)$$
$$\varepsilon_{m\phi}^2 = \frac{d_{mn}^2}{4} + R^2 - d_{mn}R\cos(\phi - \beta_{mn})$$
$$\varepsilon_{n\phi}^2 = \frac{d_{mn}^2}{4} + R^2 + d_{mn}R\cos(\phi - \beta_{mn}). \tag{7}$$

The integration of (6) can be simplified by assuming $T \gg \delta_{pq}$ and $R \gg d_{mn}$ and by using the approximation $\sqrt{1+x} \approx 1 + x/2$. Thus, the equations in (7) simplify to

$$\varepsilon_{\theta p} \approx T - \frac{\delta_{pq}}{2} \cos(\alpha_{pq} - \theta)$$

$$\varepsilon_{\theta q} \approx T + \frac{\delta_{pq}}{2} \cos(\alpha_{pq} - \theta)$$

$$\varepsilon_{m\phi} \approx R - \frac{d_{mn}}{2} \cos(\phi - \beta_{mn})$$

$$\varepsilon_{n\phi} \approx R + \frac{d_{mn}}{2} \cos(\phi - \beta_{mn}). \quad (8)$$

Many different scatterer distributions have been proposed in the literature, such as the uniform, Gaussian, wrapped Gaussian, and the cardioid pdfs. In this paper, the von Mises probability density function (pdf) [23] is used, which approximates many of these distributions and provides mathematical convenience leading to closed-form solutions for many problems. In [23], it was shown that this pdf provides a good fit to measured results. The von Mises pdf is defined as [23]

$$p(\theta) = \frac{1}{2\pi I_0(\kappa)} \exp[\kappa \cos(\theta - \mu)], \quad \theta \in [-\pi, \pi). \quad (9)$$

Here, $I_0(\cdot)$ is the modified Bessel function of the first kind of order zero, $\mu \in [-\pi, \pi)$ is the mean angle at which the scatterers are distributed on the ring, and κ controls the spread of scatterers around this mean. When $\kappa = 0$, $p(\theta) = 1/2\pi$ is a uniform distribution and one has isotropic scattering. As κ increases, the scatterers become more clustered around μ and the scattering becomes increasingly nonisotropic.

By grouping the terms in (6) into those containing θ and those containing ϕ, the double integral can be calculated as the product of two single integrals corresponding to the transmit and receive antenna correlations, $\rho_{p,q}^T$ and $\rho_{m,n}^R(\tau)$, respectively. Note that the transmit antenna correlation is independent of τ. Separable transmit and receive antenna correlations were also used in [10], [11], [16], and [20]. Thus, the space–time cross-correlation function can be expressed as

$$\rho_{mp,nq}(\tau) = \rho_{p,q}^T \cdot \rho_{m,n}^R(\tau). \quad (10)$$

Let $a = 2\pi f_D \tau$, $b_{pq} = 2\pi \delta_{pq}/\lambda$, and $c_{mn} = 2\pi d_{mn}/\lambda$. Now, substituting $p(\theta)$ and $p(\phi)$ with (9), using the approximate expressions in (8) and applying some common trigonometric identities, (6) can be rewritten as

$$\rho_{p,q}^T \approx \frac{1}{2\pi I_0(\kappa_T)}$$
$$\times \int_{-\pi}^{\pi} \exp\{(jb_{pq} \cos\alpha_{pq} + \kappa_T \cos\mu_T)$$
$$\times \cos\theta + (jb_{pq} \sin\alpha_{pq}$$
$$+ \kappa_T \sin\mu_T) \sin\theta\} d\theta \quad (11)$$

$$\rho_{m,n}^R(\tau) \approx \frac{1}{2\pi I_0(\kappa_R)}$$
$$\times \int_{-\pi}^{\pi} \exp\{(jc_{mn} \cos\beta_{mn} - ja \cos\gamma + \kappa_R \cos\mu_R)$$
$$\times \cos\phi + (jc_{mn} \sin\beta_{mn} - ja \sin\gamma$$
$$+ \kappa_R \sin\mu_R) \sin\phi\} d\phi. \quad (12)$$

Closed-form expressions for (11) and (12) can be calculated using the integral [37, eq. 3.338-4]

$$\int_{-\pi}^{\pi} e^{x \cos z + y \sin z} dz = 2\pi I_0(\sqrt{x^2 + y^2}). \quad (13)$$

Using (13), closed-form expressions for the transmit and receive antenna correlations are given by

$$\rho_{p,q}^T \approx \frac{1}{I_0(\kappa_T)}$$
$$\times I_0\left\{[\kappa_T^2 - b_{pq}^2 + 2j\kappa_T b_{pq} \cos(\alpha_{pq} - \mu_T)]^{\frac{1}{2}}\right\} \quad (14)$$

$$\rho_{m,n}^R(\tau) \approx \frac{1}{I_0(\kappa_R)}$$
$$\times I_0\left\{[\kappa_R^2 - a^2 - c_{mn}^2 + 2ac_{mn} \cos(\beta_{mn} - \gamma)\right.$$
$$+ 2j\kappa_R c_{mn} \cos(\beta_{mn} - \mu_R)$$
$$\left. - 2ja\kappa_R \cos(\gamma - \mu_R)]^{\frac{1}{2}}\right\}. \quad (15)$$

The cross-correlation function obtained here is in a compact closed form and one can easily generate new correlation results for different configurations as opposed to simulation-based models [9] where lengthy simulations are required.

In order to validate this channel model, one should ideally compare these results to field measurements. Because this model is very general, field measurements would need to be averaged over a range of environments. To the extent of the authors' knowledge, such results are currently not available in the literature for comparison.

In Section IV, the cross-correlation function (10), (14), (15) derived in this section is compared to the correlation results obtained from the geometric model discussed in Section II to assess the validity of the derivation. Good agreement between the geometric model and the derived cross-correlation function is observed.

The validity of this channel model is assessed by comparing the derived correlation results with existing channel models in the literature. The transmit antenna correlation (14) is a special case of the receive antenna correlation (15) for the case of $\tau = 0$. For this reason only, (15) will be compared with existing models.

For the case of a single receive antenna $(d_{mn} = 0)$ and isotropic scattering $(\kappa_R = 0)$, (15) reduces to Clarke's model for temporal correlation $J_0(2\pi f_D \tau)$ [22]. Here, $J_0(\cdot)$ is the zeroth-order Bessel function of the first kind. When there is non-

isotropic scattering around the user ($\kappa_R \neq 0$) and $\gamma = \pi$ (15) simplifies to

$$\frac{I_0\left(\sqrt{\kappa_R^2 - 4\pi^2 f_D^2 \tau^2 + 4\pi j f_D \tau \kappa_R \cos\mu_R}\right)}{I_0(\kappa_R)} \qquad (16)$$

which is the temporal correlation model of [23, eq. 2], which demonstrated good agreement with measured results.

For the case of multiple antennas at the receiver where a uniform linear array is used, (15) reduces to Lee's spatio–temporal model [24, Sec. VI], which assumes isotropic scattering around the user. This result is obtained by setting $\kappa_R = 0$, $\beta_{mn} = \pi$, and $f_D = -f_D$, which gives

$$J_0\left(\sqrt{a^2 + c_{mn}^2 + 2ac_{mn}\cos\gamma}\right). \qquad (17)$$

For nonisotropic scattering around the user with $\beta_{mn} = \pi$ and $f_D = -f_D$, (15) can be reduced to the spatio–temporal model of [28, eq. 3] as

$$\frac{1}{I_0(\kappa_R)} \times I_0 \left\{ \left[\kappa_R^2 - a^2 - c_{mn}^2 - 2ac_{mn}\cos\gamma \right.\right.$$
$$\left.\left. -2j\kappa_R c_{mn}\cos\mu_R - 2ja\kappa_R\cos(\mu_R - \gamma)\right]^{\frac{1}{2}}\right\} \qquad (18)$$

which was shown to agree well with correlation results published in the literature.

IV. Simulation Results for the Outage Capacity

In this section, the generation of the jointly correlated variates is described, the calculation of the outage capacity is discussed, and simulation results for the outage capacity of the spatially and temporally correlated MIMO channel are presented.

A. Generation of the Correlated Variates

The generation of correlated variates with the joint space–time cross-correlation derived in Section III is described in this section. A direct approach is to linearly transform sequences of uncorrelated variates using the square root of desired correlation matrix. This method is computationally intensive and not feasible for long sequences. For example, if N symbols are transmitted from each antenna in a single frame and $M = n_T n_R$, the computational complexity required to calculate the square root of the $NM \times NM$ correlation matrix using Cholesky reduction is $O((NM)^3)$ and to generate each frame of correlated variates is $O((NM)^2)$.

Previous methods used to efficiently generate spatially and temporally correlated fading processes generated independent fading processes with the desired autocorrelation function (ACF), which were then multiplied by a coloring matrix to obtain the desired cross-correlation function (CCF). This method of generation is only suitable when the temporal and spatial correlation statistics are separable. In [30], the vector autoregressive (AR) stochastic model of [38] was generalized to multiple channels to generate Rayleigh-fading processes with specified ACFs and CCFs.

The correlation function in this paper is complex and has joint statistics. For this reason, the AR model for variates with correlated quadrature components [30] is used. The complexity of the AR model can be reduced because the transmit and receive an-

tenna correlation functions are separable. Note that the transmit antenna correlation function describes spatial correlation only while the receive antenna correlation function jointly describes spatial and temporal correlation.

The following process is followed to generate the spatially and temporally correlated variates. For each time instance t, an $n_R \times n_T$ matrix $\boldsymbol{U}_t$ of independent zero mean complex Gaussian-random variates with unit variance is generated. The $n_R \times n_T$ matrix $\boldsymbol{X}_t$ with the desired transmit antenna correlation is generated by

$$\boldsymbol{X}_t = \boldsymbol{U}_t\sqrt{\boldsymbol{\Sigma}_T} \qquad (19)$$

where $\boldsymbol{\Sigma}_T$ is the $n_T \times n_T$ transmit antenna correlation matrix with elements $\rho_{p,q}^T$, calculated using (14). The matrix $\boldsymbol{X}_t$ is then used as the input to the vector AR stochastic model [30, Sec. 3-B] where (15) is used to calculate the required space–time correlation matrix.

B. Outage Capacity of the MIMO Channel

In the system of interest, the transmitted frame spans a fixed number of symbols, which generally occurs when delay constraints are imposed, such as in speech-transmission systems. In this case, a capacity in the Shannon sense does not exist with nonzero probability. For this reason, the outage capacity [1], [7], [39] is employed, which has been used to study the capacity of many communication systems. The outage capacity C_{out} is associated with an outage probability P_{out}, which gives the probability that the channel capacity C falls below C_{out}. This can be expressed mathematically as

$$P_{\text{out}} = P(C < C_{\text{out}}). \qquad (20)$$

The normalized capacity C_t for a particular realization $\boldsymbol{H}_t$ of a MIMO channel at time t is expressed as [1], [2]

$$C_t = \log_2 \det\left(\boldsymbol{I}_{n_R} + \frac{\rho}{n_T}\boldsymbol{H}_t\boldsymbol{H}_t^\dagger\right) \text{ bps/Hz} \qquad (21)$$

where $\dagger$ is the transpose conjugate and $\det(\cdot)$ is the matrix determinant, $\boldsymbol{I}_{n_R}$ is the $n_R \times n_R$ identity matrix, and ρ is the average signal-to-noise ratio (SNR) at each receive antenna. The capacity of a frame comprising N symbols is given by [39]

$$C = \frac{1}{N}\sum_{t=1}^{N} C_t \text{ bps/Hz}. \qquad (22)$$

C. Simulation Results

In this section, the effect of spatial and temporal correlation on the outage capacity of the presented MIMO channel is investigated. In all cases, the outage capacity C_{out} is calculated for a 1% outage probability. The expressions derived for the correlation at the transmitter and receiver in (14) and (15) can be applied to any array configuration. Here, uniform linear arrays (ULAs) are considered where the antenna spacing at the transmitter and receiver is given by δ and d, respectively. The angle of the transmit and receive antenna arrays is given by α and β, respectively. It is assumed that the local scatterers are centered around the x-axis facing the opposite antenna array. For this reason, $\mu_T = 0°$ and $\mu_R = 180°$.
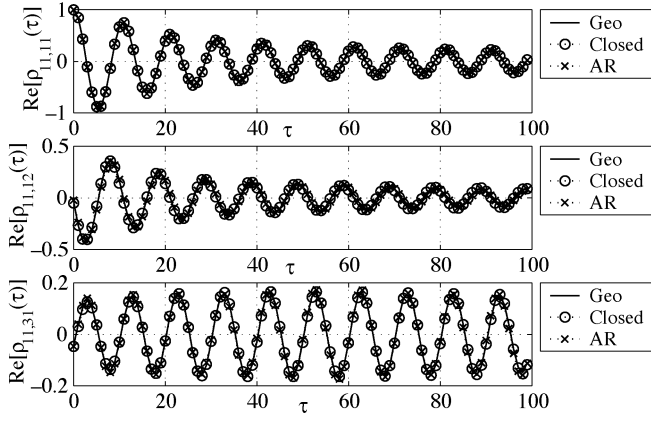
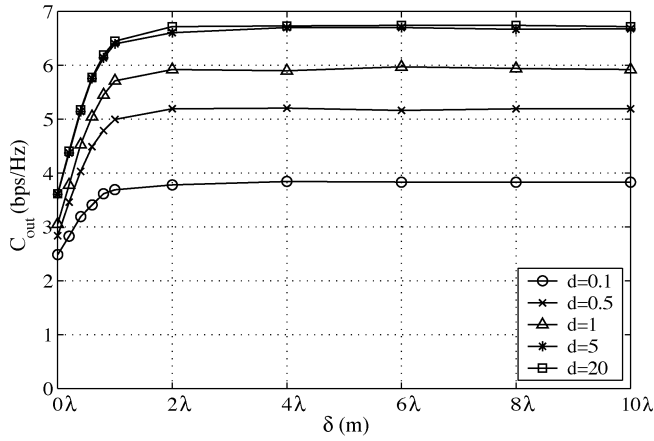Fig. 2. ACFs and CCFs for the geometric model (Geo), the closed-form CCF (Closed), and the AR model (AR).

Fig. 3. Capacity dependence on the transmitter and receiver antenna spacing (δ, d).

Fig. 4. Capacity dependence on the transmitter and receiver array angle from the x-axis (α, β).

Fig. 5. Capacity dependence on the degree of local scattering at the transmitter and receiver (κ_T, κ_R).

Unless indicated otherwise, the following parameters are used. The carrier frequency is set to 1 GHz, which corresponds to a carrier wavelength λ of 0.3 m. The SNR ρ is set to 10 dB and the frame length N is set to 100. The number of transmit and receive antennas is set to 3, i.e., $n_T = n_R = 3$ and the antenna arrays have $\delta = d = \lambda$ and $\alpha = \beta = 45°$. The normalized Doppler frequency f_D is set to 0.1 and the receiver is moving at an angle of $\gamma = 20°$. The degree of local scattering at the transmitter and receiver is $\kappa_T = \kappa_R = 10$. The order of the AR model is 80.

In order to assess the accuracy of the derived CCF (10) and the AR model, these cross-correlations are compared to those obtained from the geometric model shown in Fig. 1. Equation (3) is used to calculate the path gains of the geometric model using the parameters $K = L = 10$, $T = R = 10$ m, and $D = 1000$ m. The scatterers are distributed around the transmit and receive antenna arrays according to the von Mises distribution (9). In all cases, the parameters described previously are used. The results are illustrated in Fig. 2, where good agreement of the closed-form CCF and the AR model with the geometric model is observed.

In Fig. 3, the capacity dependence on the transmitter and receiver antenna spacing is illustrated. Increasing δ beyond 2λ and d beyond 5λ has a negligible effect on capacity. A larger
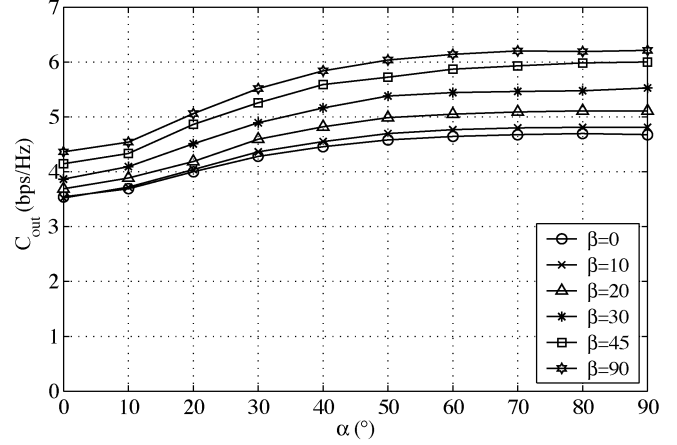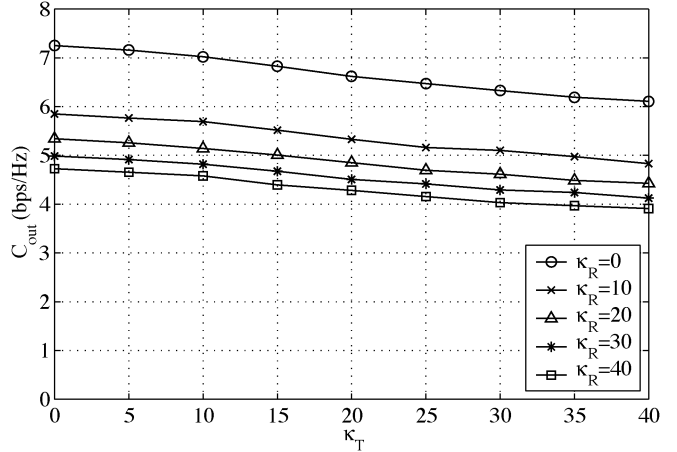
antenna spacing is thus required at the receiver to achieve maximum capacity. This is because the receiver is moving and, for this reason, a larger antenna spacing is required to overcome the temporal correlation. It is also observed that a reasonable antenna spacing at both ends of the radio link is necessary to achieve maximum capacity.

The influence of the transmitter and receiver array angle is studied in Fig. 4. The change in capacity is greatest when the antenna array is between $10°$ and $60°$. Note that the capacity achieved for $\alpha = \beta = 45°$ is only 0.6 bps/Hz lower than the maximum capacity achieved when $\alpha = \beta = 90°$.

The effect of nonisotropic scattering is observed in Fig. 5. The capacity decreases as the scattering becomes more nonisotropic, which corresponds to an increase in κ_T and κ_R. The capacity is more sensitive to a change in κ_R than κ_T where a capacity gain of 2.5 bps/Hz is obtained for a change in κ_R from 0 to 40 and only 1 bps/Hz for the same change in κ_T. This is due to the movement of the receiver where the amount temporal correlation is also dependent on κ_R.

In Figs. 3–5, it is shown that as the spatial correlation at either the transmitter or receiver increases, the capacity decreases. In all cases, optimizing the parameters at only one end of the radio
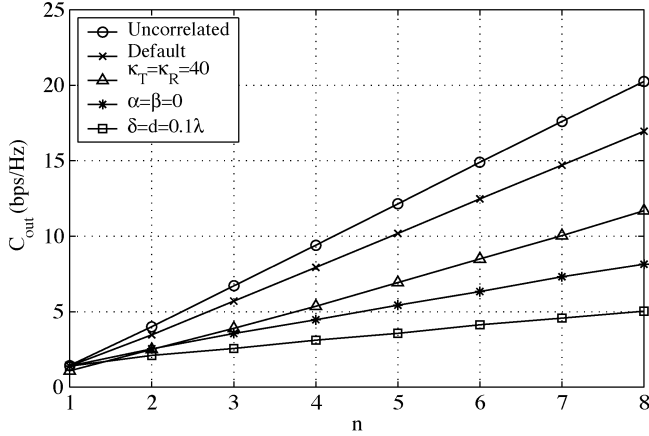
Fig. 6. Capacity dependence on the number of transmit and receive antennas (n) for varying degrees of spatial correlation.
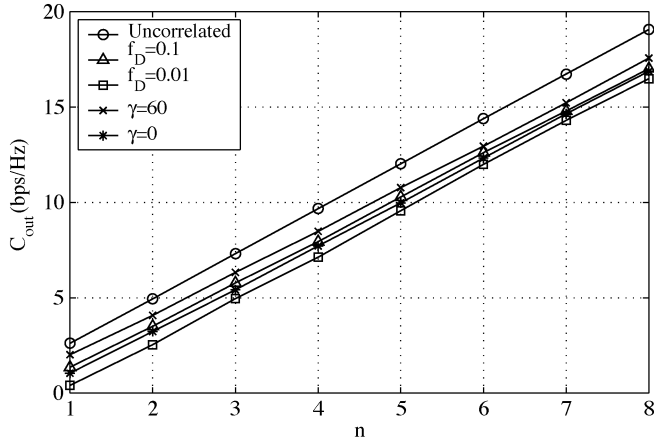

Fig. 7. Capacity dependence on the number of transmit and receive antennas (n) for varying degrees of temporal correlation.

link is not sufficient to ensure maximum capacity, thus both ends of the radio link must be considered.

In Figs. 6 and 7, the outage capacity is plotted with respect to n, which describes a system with n transmit and n receive antennas. In Fig. 6, the capacity is given for various degrees of spatial correlation. The system described at the beginning of this section is denoted by "Default" and the case of no spatial correlation is denoted by "Uncorrelated." The remaining curves give the capacity of the default system with various parameters modified, as indicated in the legend. An important result here is that capacity always increases linearly with n despite the presence of spatial and temporal correlation. Only the slope of the capacity curve is reduced as the spatial correlation increases.

The effect of temporal correlation is investigated in Fig. 7 by varying the normalized Doppler frequency f_D and the receiver direction γ. The case of temporally uncorrelated fading is shown and denoted by "Uncorrelated." It is observed that an increase in Doppler frequency results in an increase in capacity due to the decrease in temporal correlation. Increasing γ, resulting in the receiver moving more toward the transmitter, also causes an increase in capacity. Unlike the effect of spatial correlation, an increase in temporal correlation does not effect the slope or linearity of the capacity curve with respect to n, but results in a downward shift of the capacity curve.

V. ANALYTICAL EXPRESSIONS FOR THE ERGODIC CAPACITY

Both the outage and ergodic capacity have been used as capacity measures for the MIMO channel, however, the latter is less complicated to study analytically. The ergodic capacity measure is generally applied when the channel is memoryless, has no delay constraints, and the transmission time is long enough to reveal the long-term ergodic properties of the channel. The ergodic capacity is not affected by the temporal correlation, as this effect is averaged out when the transmission time is long. For this reason, only spatial correlation at the transmitter and receiver is considered.

In this section, analytical expressions are derived for the ergodic capacity of a MIMO channel with spatial correlation at one end and both ends of the radio link. This derivation is very general as it is based on the transmit and receive antenna correlation matrices. The simpler case of spatial correlation at one end of the radio link is considered first and the more complicated case of spatial correlation at both ends of the radio link is dealt with next. Throughout this analysis, it is assumed that $n_T \geq n_R$, although the analysis can be easily modified to consider the case where $n_T < n_R$.

The ergodic capacity of a MIMO channel is defined as the expectation of the capacity over time. To simplify the notation used in this section, the time index t in (21) is dropped and the ergodic capacity is expressed as [1]

$$E[C] = E\left[\log_2 \det\left(\boldsymbol{I}_{n_R} + \frac{\rho}{n_T}\boldsymbol{H}\boldsymbol{H}^\dagger\right)\right]. \qquad (23)$$

This can be rewritten in terms of the eigenvalues $\lambda_1, \ldots, \lambda_{n_R}$ of $\boldsymbol{A} = \boldsymbol{H}\boldsymbol{H}^\dagger$ where

$$E[C] = E\left[\sum_{i=1}^{n_R}\log_2\left(1 + \frac{\rho}{n_T}\lambda_i\right)\right]. \qquad (24)$$

The eigenvalues of $\boldsymbol{A}$ are nonnegative real numbers as $\boldsymbol{A}$ is Hermitian. Let $p(\underline{\lambda})$ denote the distribution of the eigenvalues of $\boldsymbol{A}$ where $\underline{\lambda} = [\lambda_1, \ldots, \lambda_{n_R}]$. The ergodic capacity can now be calculated by integrating over $p(\underline{\lambda})$ and is given by

$$E[C] = \int_0^\infty \cdots \int_0^\infty \sum_{i=1}^{n_R}\log_2\left(1 + \frac{\rho}{n_T}\lambda_i\right) p(\underline{\lambda})d\underline{\lambda}. \qquad (25)$$

By integrating over the distribution of the eigenvalues of $\boldsymbol{A}$, as opposed to the distribution of $\boldsymbol{H}$, the order of integration is reduced from $2n_T n_R$ to n_R.

In this paper, the $n_T \times n_T$ transmit antenna correlation matrix is denoted by $\boldsymbol{\Sigma}_T$ and the $n_R \times n_R$ receive antenna correlation matrix is denoted by $\boldsymbol{\Sigma}_R$.

A. Spatial Correlation at the Receiver

The distribution of the eigenvalues of $\boldsymbol{A}$ is presented here for the case of spatial correlation at the receiver. This analysis can be easily modified to study spatial correlation at the transmitter by interchanging the subscripts T and R. Here, $\boldsymbol{H}$ is zero mean and normally distributed with independent columns and covariance matrix $\boldsymbol{\Sigma}_R$.

When $n_T \geq n_R$, the matrix $\boldsymbol{A}$ has a Wishart distribution with n_T degrees of freedom [40], [41]. However, when $n_T < n_R$, $\boldsymbol{A}$

is singular and no distribution for $\boldsymbol{A}$ exists. In [41], the distribution of the ordered eigenvalues of the complex Wishart distribution was given. By scaling this distribution by the factor $1/n_R!$, the distribution of the unordered eigenvalues of a complex Wishart distributed matrix $\boldsymbol{A}$ is given by

$$
p(\underline{\lambda}) = C_1 \cdot {}_0\tilde{F}_0\left(-\boldsymbol{\Sigma}_R^{-1}, \boldsymbol{\Lambda}\right) \cdot \prod_{i=1}^{n_R} \lambda_i^{n_T - n_R} \cdot \prod_{i<j}^{n_R} (\lambda_i - \lambda_j)^2
$$

$$
C_1 = \frac{\pi^{n_R(n_R-1)} \det(\boldsymbol{\Sigma}_R)^{-n_T}}{n_R! \tilde{\Gamma}_{n_R}(n_T) \tilde{\Gamma}_{n_R}(n_R)}
$$

$$
\tilde{\Gamma}_m(n) = \pi^{\frac{m(m-1)}{2}} \prod_{i=1}^{m} \Gamma(n - i + 1). \tag{26}
$$

Here, ${}_0\tilde{F}_0(\cdot, \cdot)$ is the hypergeometric function of two matrix arguments, $\tilde{\Gamma}_m(n)$ is the complex multivariate gamma function, $\Gamma(\cdot)$ is the gamma function, and $\boldsymbol{\Lambda} = \mathrm{diag}(\lambda_1, \ldots, \lambda_{n_R})$. This expression would be straightforward to evaluate if it were not for the hypergeometric function of matrix argument, which is generally expressed as a series expansion of zonal polynomials [40], [41]. However this formulation is not practical for numerical work, as zonal polynomials are well known for being extremely difficult to compute and the series expansion is slow to converge. A more tractable formulation was proposed in [42], where the hypergeometric function of two matrix arguments was computed in terms of classical hypergeometric functions as

$$
{}_0\tilde{F}_0(\boldsymbol{S}, \boldsymbol{T}) = \frac{\det\left({}_0F_0(s_i t_j)\right)}{V(\boldsymbol{S}) V(\boldsymbol{T})} \prod_{j=1}^{n} (j-1)!
$$

$$
\det\left({}_0F_0(s_i t_j)\right) = \det \begin{pmatrix} {}_0F_0(s_1 t_1) & \cdots & {}_0F_0(s_1 t_n) \\ \vdots & \ddots & \vdots \\ {}_0F_0(s_n t_1) & \cdots & {}_0F_0(s_n t_n) \end{pmatrix}
$$

$$
V(\boldsymbol{S}) = \prod_{i<j}^{n} (s_i - s_j)
$$

$$
V(\boldsymbol{T}) = \prod_{i<j}^{n} (t_i - t_j) \tag{27}
$$

where $\boldsymbol{S}$ and $\boldsymbol{T}$ are $n \times n$ Hermitian matrices with real eigenvalues $s_1, \ldots, s_n$ and $t_1, \ldots, t_n$, respectively. The function ${}_0F_0(x) = \exp(x)$ is the classical hypergeometric function. This formulation requires that the eigenvalues of the matrices $\boldsymbol{S}$ and $\boldsymbol{T}$ are unequal. This problem is partially avoided when (27) is substituted into (26) as $V(\boldsymbol{\Lambda})$ divides into the second product term of (26). The distribution of the unordered eigenvalues of $\boldsymbol{A}$ can now be calculated as

$$
p(\underline{\lambda}) = C_2 \cdot \det\left(\exp(\lambda_i \sigma_j)\right) \cdot \prod_{i=1}^{n_R} \lambda_i^{n_T - n_R} \cdot \prod_{i<j}^{n_R} (\lambda_i - \lambda_j)
$$

$$
C_2 = \frac{\pi^{n_R(n_R-1)} \det(\boldsymbol{\Sigma}_R)^{-n_T} \prod_{j=1}^{n_R}(j-1)!}{n_R! \tilde{\Gamma}_{n_R}(n_T) \tilde{\Gamma}_{n_R}(n_R) V\left(-\boldsymbol{\Sigma}_R^{-1}\right)} \tag{28}
$$

where the σ_js are the eigenvalues of $-\boldsymbol{\Sigma}_R^{-1}$. The eigenvalues of $\boldsymbol{\Sigma}_R$ are restricted to be unequal, which is generally the case for correlation matrices. The ergodic capacity is calculated by substituting (28) into (25) and evaluating the integral numerically.

B. Spatial Correlation at the Transmitter and Receiver

In this section, the distribution of the eigenvalues of $\boldsymbol{A}$ is presented where spatial correlation at the transmitter and receiver is accounted for. In this case, $\boldsymbol{H}$ is zero mean and normally distributed where $\boldsymbol{\Sigma}_T$ and $\boldsymbol{\Sigma}_R$ are the covariance matrices of the rows and columns, respectively.

The distribution of $\boldsymbol{A}$ is a special case of the quadratic form of normal vectors and has been studied by a number of authors [43], [44]. In [44], the distribution of the eigenvalues of the quadratic form of complex normal vectors was derived. The distribution of the unordered eigenvalues of $\boldsymbol{A}$ is obtained by setting the constant matrices in [44, Sec. 8] to identity matrices and scaling the distribution by $1/n_R!$ such that

$$
p(\underline{\lambda}) = C_3 \cdot {}_0\tilde{F}_0\left(\boldsymbol{\Sigma}_T^{-1}, \boldsymbol{\Lambda}, -\boldsymbol{\Sigma}_R^{-1}\right) \cdot \prod_{i=1}^{n_R} \lambda_i^{n_T - n_R}
$$

$$
\cdot \prod_{i<j}^{n_R} (\lambda_i - \lambda_j)^2
$$

$$
C_3 = \frac{\pi^{n_R(n_R-1)} \det(\boldsymbol{\Sigma}_T)^{-n_R} \det(\boldsymbol{\Sigma}_R)^{-n_T}}{n_R! \tilde{\Gamma}_{n_R}(n_T) \tilde{\Gamma}_{n_R}(n_R)} \tag{29}
$$

where ${}_0\tilde{F}_0(\cdot, \cdot, \cdot)$ is the hypergeometric function of three matrix arguments. This function can be evaluated using a series expansion of zonal polynomials but, as discussed previously, this formulation is not practical for numerical work. As far as the authors are aware, no formulation for this function exists, which can be evaluated numerically with realizable complexity.

VI. ANALYTICAL RESULTS FOR THE ERGODIC CAPACITY

In this section, the analytical expression derived in Section V-A for the ergodic capacity of a MIMO channel with spatial correlation at the receiver is compared to simulation results. The system investigated here uses the simulation parameters described in Section IV, except that spatial correlation at the transmitter and temporal correlation at the receiver is ignored. Thus, $\boldsymbol{\Sigma}_T$ is set to the identity matrix and the elements of $\boldsymbol{\Sigma}_R$ are set to $\rho_{m,n}^R(0)$ (15).

The analytical expression (25) with (28) substituted for $p(\underline{\lambda})$ is evaluated using numerical integration where a multidimensional adaptive step-size technique is used with limits of integration of 0 and 100 for each dimension. The simulation results are generated using Monte Carlo methods. In this channel model, the antenna spacing, antenna array angle, and degree of nonisotropic scattering all affect the receive antenna correlation. In order to assess the accuracy of the analytical expression, one need only vary one of these parameters. In this section, the antenna spacing is varied.

In Fig. 8, the analytical results are compared to simulation results for the ergodic capacity. In all cases, the analysis is shown to be accurate. Difficulty was experienced in obtaining analytical results for high-dimension systems with small antenna spacings. As the antenna correlation increases, the peaks in the eigenvalue distribution (28) become sharper. This point is illustrated in Figs. 9 and 10, where the distribution of the eigenvalues $p(\lambda_1, \lambda_2)$ is given for an $n = 2$ MIMO channel. When $d = \lambda$, the two peaks are small and spread out, while for a smaller
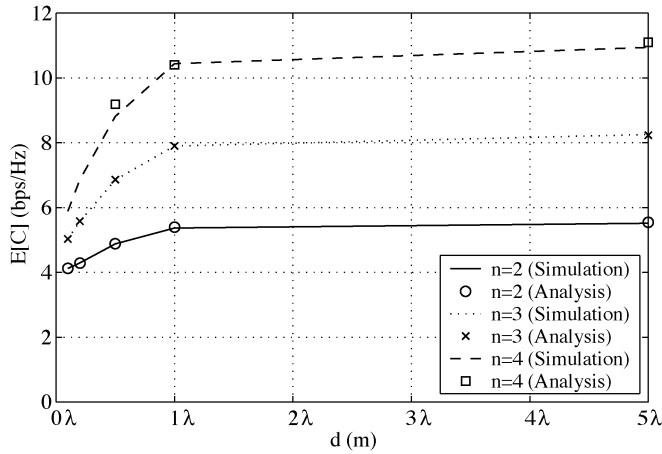
Fig. 8. Analytical and simulation results for ergodic capacity for an n transmit and n receive antenna system with receiver antenna spacing $d = 0.1\lambda, 0.2\lambda, 0.5\lambda, \lambda, 5\lambda$.
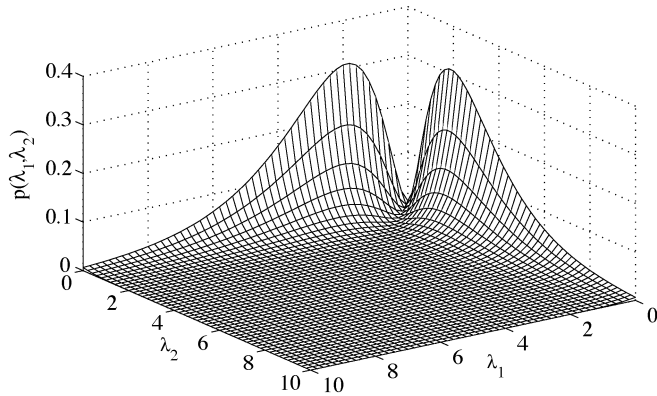

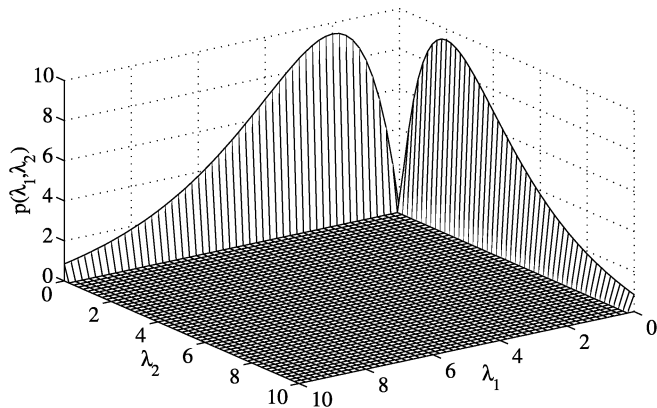Fig. 9. Distribution of the eigenvalues of $\mathbf{A}$ for $d = \lambda$.

Fig. 10. Distribution of the eigenvalues of $\mathbf{A}$ for $d = 0.1\lambda$.

spacing of $d = 0.1\lambda$, the peaks are higher and sharper due to the increase in correlation. These sharp peaks increase the computational complexity of the numerical integration as a smaller step size is required to obtain accurate results. Thus, for large-dimension systems with high spatial correlation, it is not feasible to obtain analytical results.

VII. CONCLUSION

In this paper, the outage capacity of a MIMO channel with receiver motion and nonisotropic scattering at both ends of the radio link was considered. A geometric model for this channel was presented and a closed form joint space–time CCF was derived. This derivation was shown to be accurate by comparison with correlation results obtained from the geometric model and existing models in the literature. The MIMO channel with the specified joint-correlation statistics was generated using the vector AR stochastic model.

The outage capacity of this channel was then investigated where the effects of antenna spacing and array angle, degree of nonisotropic scattering, Doppler frequency, and receiver direction were considered. It was shown that it is necessary to optimize the parameters at both ends of the radio link in order to achieve maximum capacity. Furthermore, the antenna spacing at the receiver was more critical than that at the transmitter. It was also shown that, in the presence of both spatial and temporal correlation, the capacity still scales linearly with respect to n, where n describes the case of n transmit and n receive antennas. In general, an increase in spatial correlation reduced the slope of the capacity curve while an increase in temporal correlation caused a downward shift of the capacity curve.

Analytical expressions were derived for the ergodic capacity of a MIMO channel for the cases of spatial correlation at the receiver only and spatial correlation at both the transmitter and receiver. The latter expression did not lend itself to numerical evaluation. For the case of spatial correlation at the receiver, the analytical results were shown to be accurate by comparison with simulation results. However, difficulty was experienced in evaluating the multidimensional integral for large-dimension systems with high correlation.

REFERENCES

[1] I. E. Telatar, "Capacity of Multi-Antenna Gaussian Channels," AT&T Bell Laboratories, Murray Hill, NJ, Tech. Rep. #BL0 112 170-950 615-07TM, 1995.
[2] G. J. Foschini and M. J. Gans, "On limits of wireless communications in a fading environment when using multiple antennas," *Wireless Pers. Commun.*, vol. 6, no. 3, pp. 311–335, 1998.
[3] G. J. Foschini, "Layered space–time architecture for wireless communication in a fading environment when using multiple antennas," *Bell Labs Tech. J.*, vol. 1, pp. 41–59, 1996.
[4] V. Tarokh, N. Seshadri, and A. R. Calderbank, "Space–time codes for high data rate wireless communication: Performance criterion and code construction," *IEEE Trans. Inform. Theory*, vol. 44, pp. 744–765, Mar. 1998.
[5] V. Tarokh, H. Jafarkhani, and A. R. Calderbank, "Space–time block codes from orthogonal designs," *IEEE Trans. Inform. Theory*, vol. 45, pp. 1456–1467, July 1999.
[6] D. Shiu, G. J. Foschini, M. J. Gans, and J. M. Kahn, "Fading correlation and its effect on the capacity of multielement antenna systems," *IEEE Trans. Commun.*, vol. 48, pp. 502–513, Mar. 2000.
[7] H. Bölcskei, D. Gesbert, and A. J. Paulraj, "On the capacity of OFDM-based spatial multiplexing systems," *IEEE Trans. Commun.*, vol. 50, pp. 225–234, Feb. 2002.
[8] A. Abdi and M. Kaveh, "A space–time correlation model for multielement antenna systems in mobile fading channels," *IEEE J. Select. Areas Commun.*, vol. 20, pp. 550–560, Apr. 2002.
[9] F. B.F. Boixadera Espax and J. J. Boutros, "Capacity considerations for wireless MIMO channels," in *Proc. Workshop Multiaccess, Mobility and Teletraffic for Wireless Communications*, Venice, Italy, Oct. 1999.
[10] D. Gesbert, H. Bölcskei, D. Gore, and A. Paulraj, "MIMO wireless channels: Capacity and performance prediction," in *IEEE GLOBECOM '00*, vol. 2, Nov. 2000, pp. 1083–1088.

[11] C. Chuah, D. N. C. Tse, J. M. Kahn, and R. A. Valenzuela, "Capacity scaling in MIMO wireless systems under correlated fading," *IEEE Trans. Inform. Theory*, vol. 48, pp. 637–650, Mar. 2002.

[12] J. W. Wallace and M. A. Jensen, "Spatial characteristics of the MIMO wireless channel: Experimental data acquisition and analysis," in *Proc. IEEE Int. Conf. Acoustics, Speech and Signal Processing*, vol. 4, May 2001, pp. 2497–2500.

[13] R. Stridh, B. Ottersten, and P. Karlsson, "MIMO channel capacity on a measured indoor radio channel at 5.8 GHz," in *Proc. Asilomar Conf. Signals, Systems and Computers*, vol. 1, Oct. 2000, pp. 733–737.

[14] D. P. McNamara, M. A. Beach, and P. N. Fletcher, "Experimental investigation of the temporal variation of MIMO channels," in *Proc. IEEE VTC '01*, vol. 2, Oct. 2001, pp. 1063–1067.

[15] P. Kyritsi, D. C. Cox, R. A. Valenzuela, and P. W. Wolniansky, "Correlation analysis based on MIMO channel measurements in an indoor environment," *IEEE J. Select. Areas Commun.*, vol. 21, pp. 713–720, June 2003.

[16] J. P. Kermoal, L. Schumacher, K. I. Pedersen, P. E. Mogensen, and F. Frederiksen, "A stochastic MIMO radio channel model with experimental validation," *IEEE J. Select. Areas Commun.*, vol. 20, pp. 1211–1226, Aug. 2002.

[17] C. C. Martin, J. H. Winters, and N. R. Sollenberger, "MIMO radio channel measurements: Performance comparison of antenna configurations," in *Proc. IEEE VTC '01*, vol. 2, Oct. 2001, pp. 1225–1229.

[18] P. Soma, D. S. Baum, V. Erceg, R. Krishnamoorthy, and A. J. Paulraj, "Analysis and modeling of multiple-input–multiple-output (MIMO) radio channel based on outdoor measurements conducted at 2.5 GHz for fixed BWA applications," in *Proc. IEEE ICC '02*, vol. 1, May 2002, pp. 272–276.

[19] H. Xu, M. Gans, D. Chizhik, J. Ling, P. Wolniansky, and R. Valenzuela, "Spatial and temporal variations of MIMO channels and impacts on capacity," in *Proc. IEEE ICC '02*, vol. 1, May 2002, pp. 262–266.

[20] D. Chizhik, J. Ling, P. W. Wolniansky, R. A. Valenzuela, N. Costa, and K. Huber, "Multiple-input–multiple-output measurements and modeling in Manhattan," *IEEE J. Select. Areas Commun.*, vol. 21, pp. 321–331, Apr. 2003.

[21] K. Yu and B. Ottersten, "Models for MIMO propagation channels, a review," *Wiely J. Wireless Commun. Mobile Comput.*, vol. 2, no. 7, pp. 653–666, 2002.

[22] W. C. Jakes, *Microwave Mobile Communications*. New York: Wiley, 1974.

[23] A. Abdi, J. A. Barger, and M. Kaveh, "A parametric model for the distribution of the angle of arrival and the associated correlation function and power spectrum at the mobile station," *IEEE Trans. Veh. Technol.*, vol. 51, pp. 425–434, May 2002.

[24] W. C. Y. Lee, "Level crossing rates of an equal-gain predetection diversity combiner," *IEEE Trans. Commun. Technol.*, vol. 18, pp. 417–426, 1970.

[25] R. B. Ertel, P. Cardieri, K. W. Sowerby, T. S. Rappaport, and J. H. Reed, "Overview of spatial channel models for antenna array communication systems," *IEEE Pers. Commun.*, vol. 5, pp. 10–22, Feb. 1998.

[26] J. Fuhl, A. F. Molisch, and E. Bonek, "Unified channel model for mobile radio systems with smart antennas," *Proc. Inst. Elect. Eng. Radar, Sonar, Navig.*, vol. 145, no. 1, pp. 32–41, Feb. 1998.

[27] T. A. Chen, M. P. Fitz, W. Y. Kuo, M. D. Zoltowski, and J. H. Grimm, "A space–time model for frequency nonselective Rayleigh fading channels with applications to space-time modems," *IEEE J. Select. Areas Commun.*, vol. 18, pp. 1175–1190, July 2000.

[28] A. Abdi and M. Kaveh, "A versatile spatio-temporal correlation function for mobile fading channels with nonisotropic scattering," in *Proc. IEEE Workshop Statistical Signal Array Processing*, Aug. 2000, pp. 58–62.

[29] A. F. Molisch, "A generic model for MIMO wireless propagation channels," in *Proc. IEEE ICC '02*, vol. 1, May 2002, pp. 277–282.

[30] K. E. Baddour and N. C. Beaulieu, "Accurate simulation of multiple cross-correlated fading channels," in *Proc. IEEE ICC '02*, vol. 1, May 2002, pp. 267–271.

[31] D. W. Bliss, K. W. Forsythe, and A. F. Yegulalp, "MIMO communication capacity using infinite dimension random matrix eigenvalue distributions," in *Proc. 35th Asilomar Conf. Signals, Systems and Computers*, vol. 2, Nov. 2001, pp. 969–974.

[32] L. Hanlen and M. Fu. MIMO wireless systems: Capacity limits for sparse scattering. presented at *Proc. Third Australian Communications Theory Workshop*. [Online] http://citeseer.ist.psu.edu/hanlen02mimo.html

[33] H. Ge, K. D. Wong, M. Barton, and J. C. Liberti, "Statistical characterization of multiple-input–multiple-output (MIMO) channel capacity," in *Proc. IEEE WCNC '02*, vol. 2, Mar. 2002, pp. 789–793.

[34] P. J. Smith and M. Shafi, "On a Gaussian approximation to the capacity of wireless MIMO systems," in *Proc. IEEE ICC '02*, vol. 1, May 2002, pp. 406–410.

[35] S. Loyka and A. Kouki, "New compound upper bound on MIMO channel capacity," *IEEE Commun. Lett.*, vol. 6, pp. 96–98, Mar. 2002.

[36] X. Mestre, J. R. Fonollosa, and A. Pagès-Zamora, "Capacity of MIMO channels: Asymptotic evaluation under correlated fading," *IEEE J. Select. Areas Commun.*, vol. 21, pp. 829–838, June 2003.

[37] I. S. Gradshteyn and I. M. Ryzhik, *Table of Integrals, Series and Products*, 5th ed, A. Jeffrey, Ed. San Diego, CA: Academic, 1994.

[38] K. E. Baddour and N. C. Beaulieu, "Autoregressive models for fading channel simulation," in *Proc. IEEE GLOBECOM '01*, vol. 2, Nov. 2001, pp. 1187–1192.

[39] E. Biglieri, G. Caire, and G. Taricco, "Limiting performance of block-fading channels with multiple antennas," *IEEE Trans. Inform. Theory*, vol. 47, pp. 1273–1289, May 2001.

[40] R. J. Muirhead, *Aspects of Multivariate Statistical Theory*. New York: Wiley, 1982.

[41] A. T. James, "Distributions of matrix variates and latent roots derived from normal samples," *Ann. Math. Statist.*, vol. 35, pp. 475–501, 1964.

[42] K. I. Gross and D. S. P. D. St. P. Richards, "Total positivity, spherical series, and hypergeometric functions of matrix argument," *J. Approx. Theory*, vol. 59, pp. 224–246, 1989.

[43] C. G. Khatri, "On certain distribution problems based on positive definite quadratic functions in normal vectors," *Ann. Math. Statist*, vol. 37, pp. 468–479, 1966.

[44] N. A. S. Crowther and D. J. de Waal, "On the distribution of a generalized positive semidefinite quadratic form of normal vectors," *South African Statist. J.*, vol. 7, pp. 119–127, 1973.

Geoffrey J. Byers (S'02) received the B.Sc. and M.Sc. degrees in electronic engineering from the University of Natal, Durban, South Africa, in 1999 and 2001, respectively, and is currently working toward the Ph.D. degree.

His research interests include mulitple-input–multiple-output channels and error control coding for multiple antenna wireless communication systems.

Fambirai Takawira (M'96) received the B.Sc. degree in electrical engineering (first class Hons) from Manchester University, Manchester, U.K., in 1981 and the Ph.D. degree from Cambridge University, Cambridge, U.K., in 1984.

He currently is the Head of the School of Electrical, Electronic, and Computer Engineering at the University of Natal, Durban, South Africa. His research interests include digital communication systems and networks with an emphasis on code-division multiple-access systems.